catalysts

Supporting Information

Article

Mitigating Co Metal Particle Agglomeration and Enhancing ORR Catalytic Activity through Nitrogen-Enriched Porous Carbon Derived from Biomass

Yanling Wu [1], Qinggao Hou [1,*], Fangzhou Li [1], Yuanhua Sang [2], Mengyang Hao [1], Xi Tang [1], Fangyuan Qiu [1] and Haijun Zhang [3,*]

[1] Jinan Key Laboratory of New Energy & New Materials for Intelligent Transportation, School of Civil Engineering, Shandong Jiaotong University, Jinan 250357, China; wuyanling621@163.com (Y.W.)
[2] State Key Laboratory of Crystal Materials, Shandong University, Jinan 250100, China; sangyh@sdu.edu.cn
[3] Department of Vascular & Intervention, Tenth Peoples' Hospital of Tongji University, Shanghai 200072, China
* Correspondence: chqghou@163.com (Q.H.); zhanghaijun@tongji.edu.cn (H.Z.)

Supplementary figures

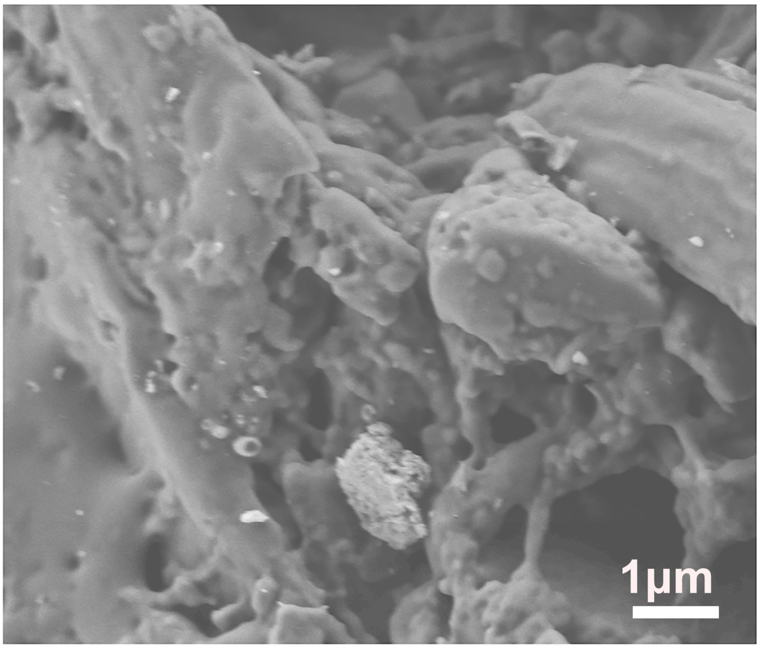

Figure S1. The SEM image of SP-C.

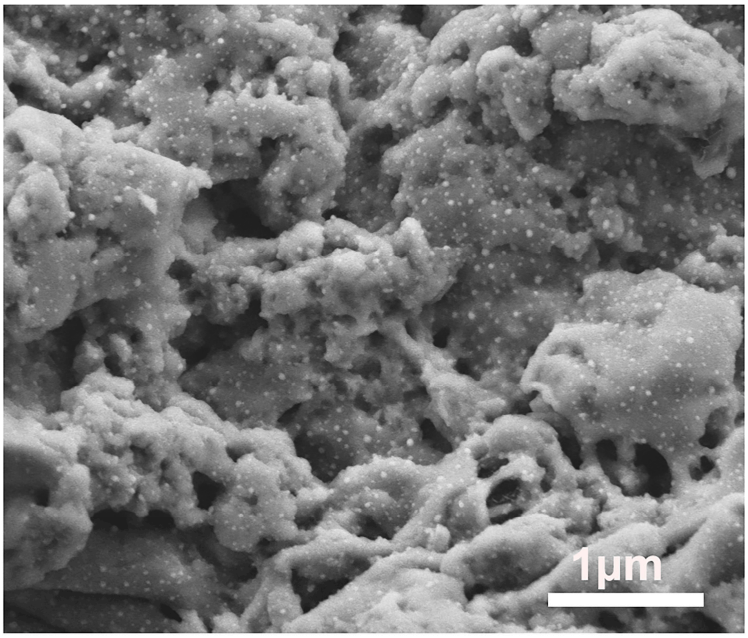

Figure S2. The SEM image of SP-C-a.

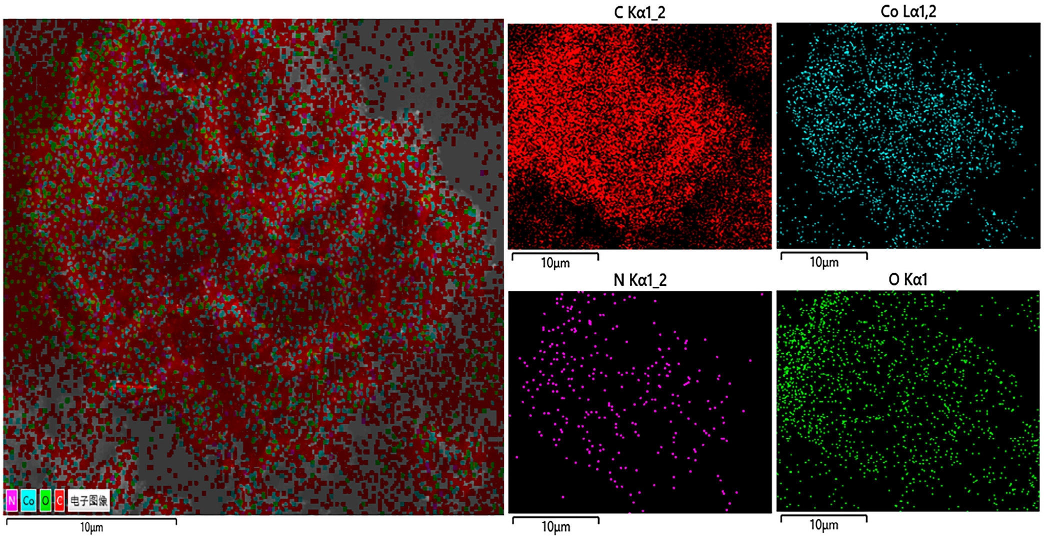

Figure S3. SEM image of Co@SP-C-a used in the EDS mapping area revealing the elemental distribution of Co, C, N, and O.

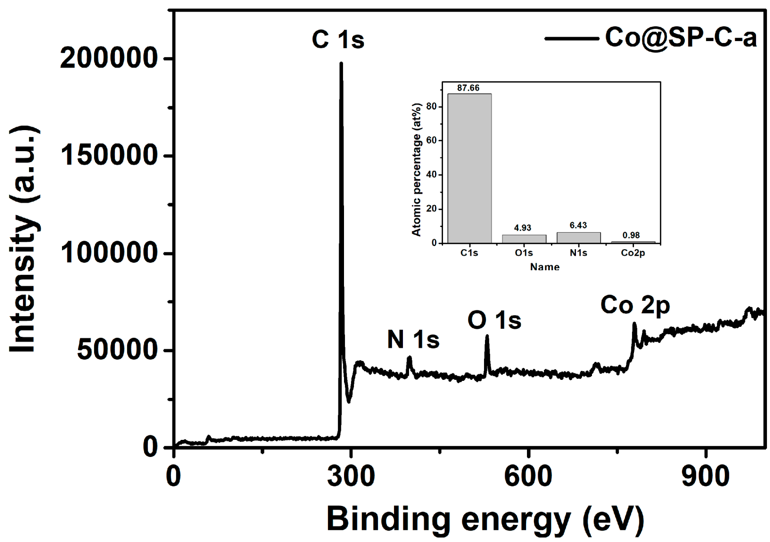

Figure S4. XPS survey spectra of Co@SP-C-a.

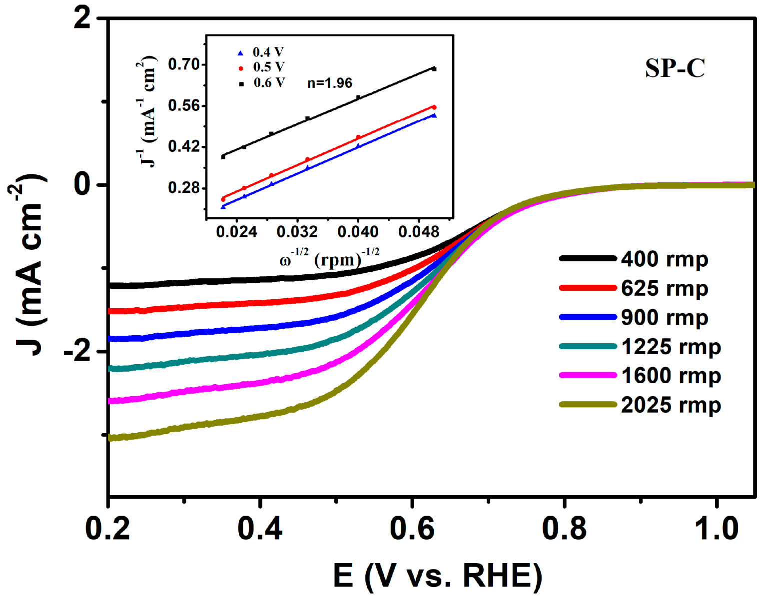

Figure S5. LSV curves of SP-C at various rotating speeds, respectively. (Inset: K–L plots of SP-C at various potentials.).

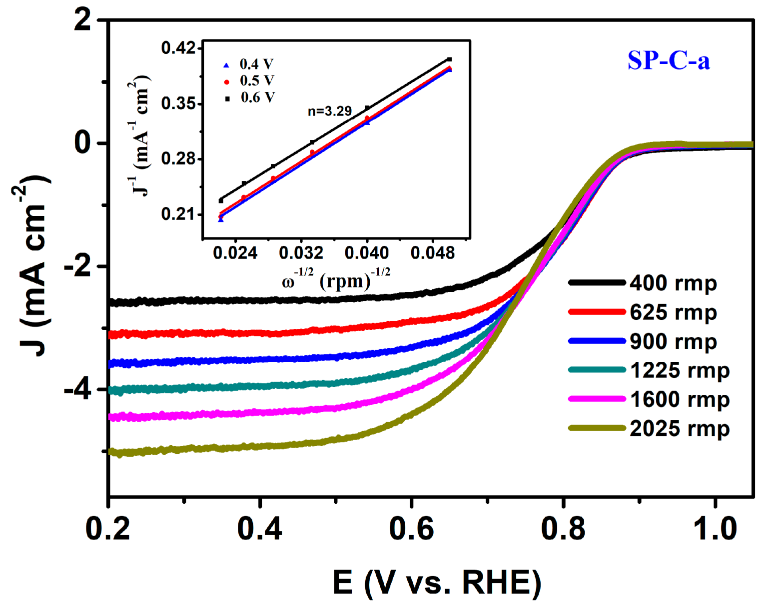

Figure S6. LSV curves of SP-C-a at various rotating speeds, respectively. (Inset: K–L plots of SP-C-a at various potentials.).

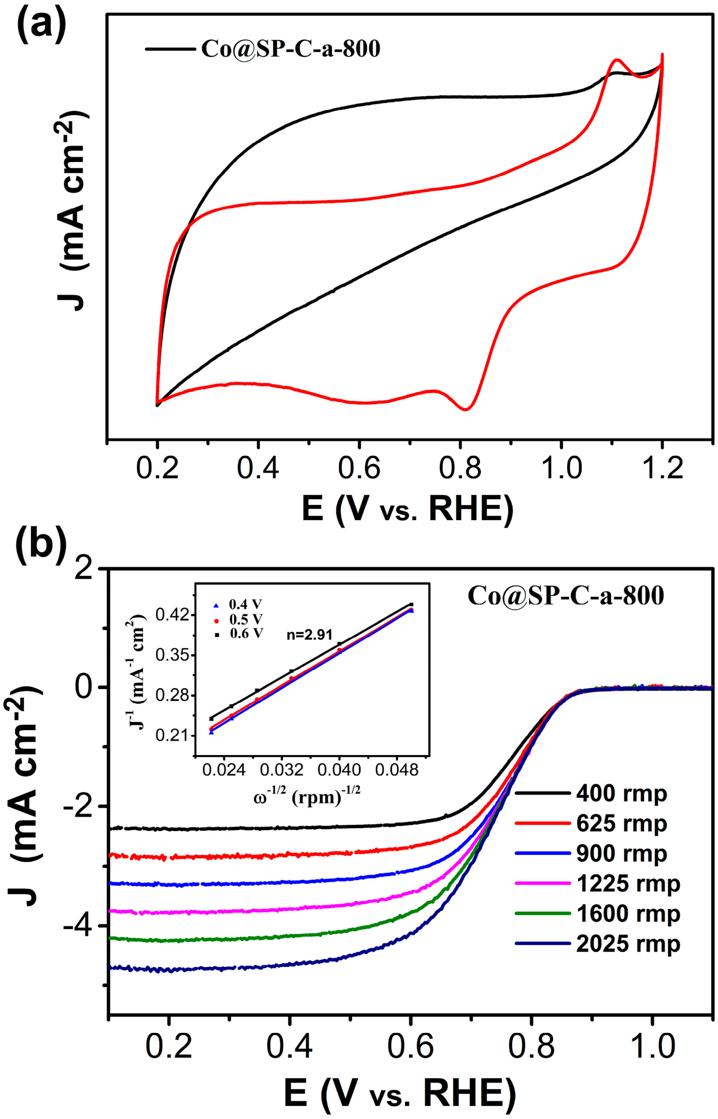

Figure S7. CV and LSV curves of SP-C-a-800 at various rotating speeds, respectively. (Inset: K–L plots of SP-C-a-800 at various potentials.).

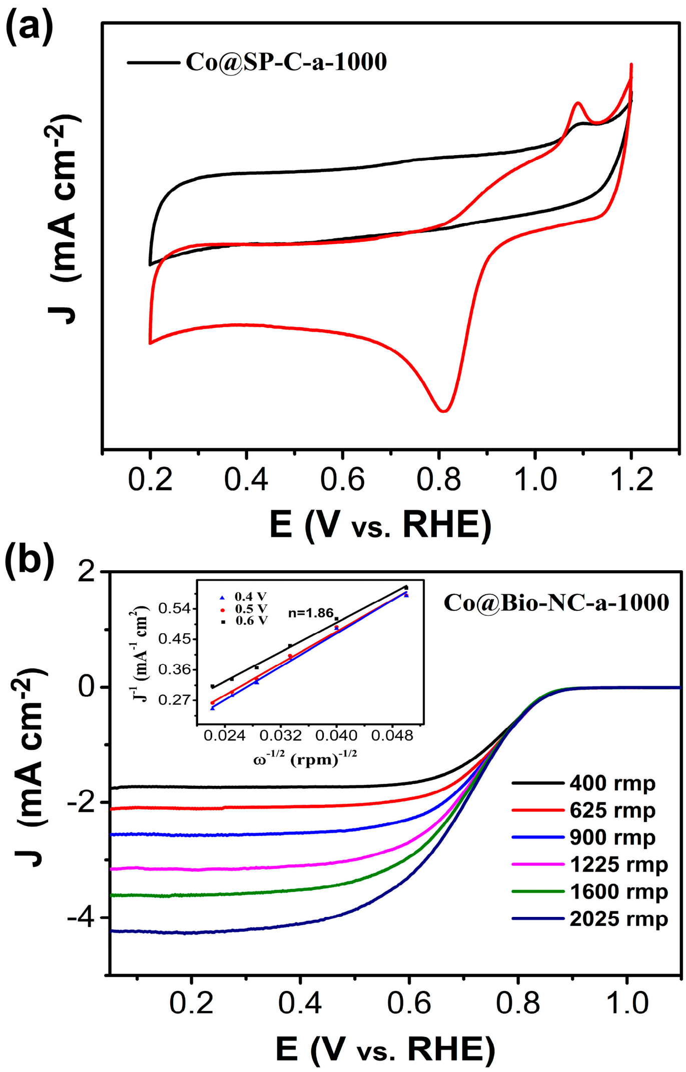

Figure S8. CV and LSV curves of SP-C-a-1000 at various rotating speeds, respectively. (Inset: K–L plots of SP-C-a-1000 at various potentials.).

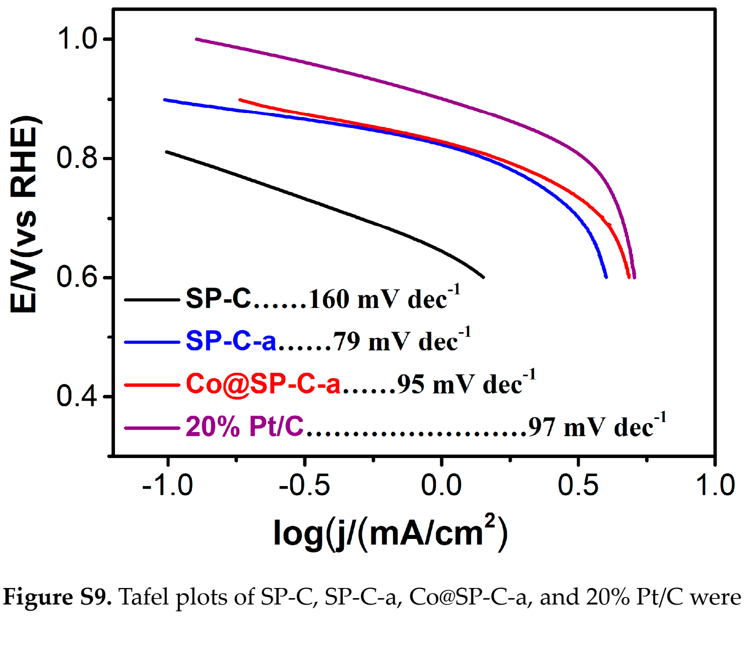

Figure S9. Tafel plots of SP-C, SP-C-a, Co@SP-C-a, and 20% Pt/C were obtained via LSV data.

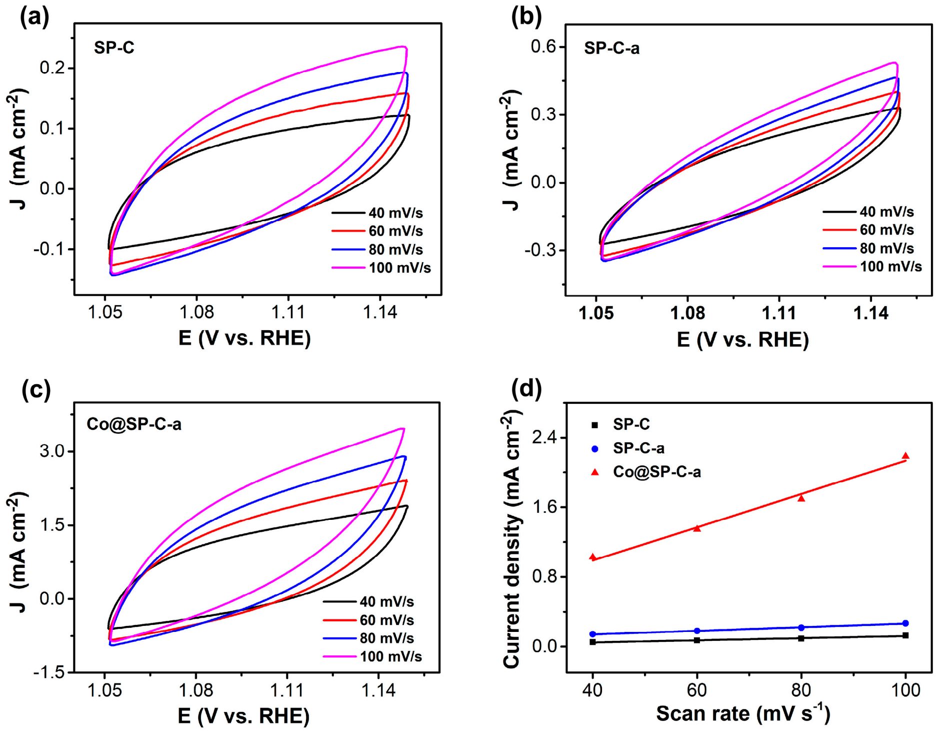

Figure S10. Cyclic voltammograms (CV) at various scan rates of (a) SP-C, (b) SP-C-a, and (c) Co@SP-C-a in 0.1 M KOH solution. (d) The electrochemical double-layer capacitance (C_{dl}) of SP-C, SP-C-a, and Co@SP-C-a in 0.1 M KOH electrolyte.

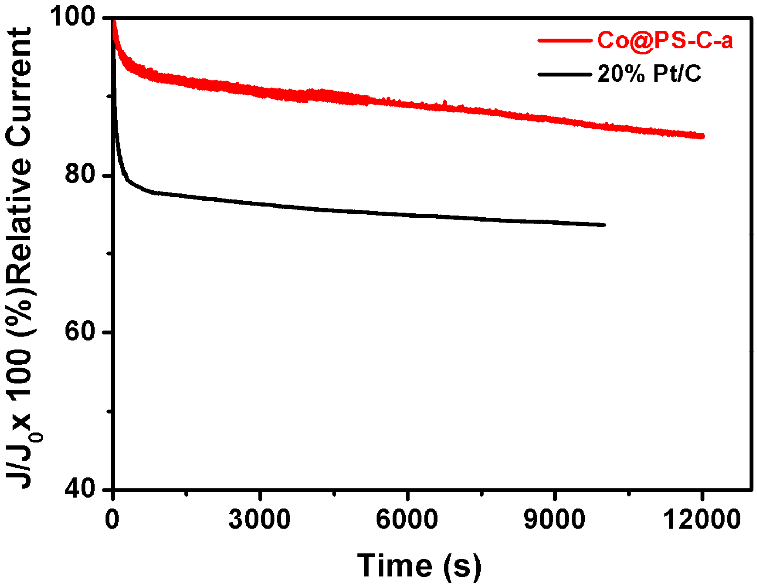

Figure S11. Amperometric i–t curves of Co@SP-C-a and 20 wt% Pt/C in O_2-saturated 0.1 M KOH solution with the rotation speed of 1600 rpm.

Table S1. The ORR performance of the SP-C, SP-C-a, Co@SP-C-a-800, Co@SP-C-a-1000, and Co@SP-C-a, in alkaline media at 1600 rpm, respectively.

Sample	E_{onset} (V)	$E_{1/2}$ (V)	J_L (mA cm^{-2})	*n*	*Tafel* (mV dec^{-1})
SP-C	0.76	0.57	2.58	1.96	160
SP-C-a	0.86	0.78	4.45	3.29	75
Co@SP-C-a-800	0.87	0.81	4.25	2.91	/
Co@SP-C-a-1000	0.85	0.83	3.62	1.86	/
Co@SP-C-a	0.89	0.81	6.13	3.96	95
20 wt% Pt/C	0.96	0.86	5.61	4.00	97

Table S2. Comparison of the ORR performance for Co@SP-C-a catalysts at 1600 rpm in 0.1 M KOH.

Catalysts	$E_{1/2}$ (V)	J_L (mA cm^{-2})	E_{onset} (V)	Tafel slope (mV dec^{-1})	*n*	Reference
Co@SP-C-a	0.83	6.13	0.89	--	3.96	This work
Co@Co_3O_4@C	0.78	4.65	0.90	--	--	*Energy Environ. Sci.*, 2015 [1]
Co@NG-acid	0.83	4.00	0.90	--	3.90	*Adv. Funct. Mater.*, 2016 [2]
Co-NC@CoP-NC	0.78	4.70	0.89	--	3.97	*J. Mater. Chem. A*, 2016 [3]
Co@Co_3O_4@PPD	0.78	4.20	0.90	--	3.78~3.96	*Small*, 2016 [4]
Co@NCNT	0.83	6.20	1.03	--	--	*J. Mater. Chem. A*, 2016 [5]
Co,N-CNF	0.85	5.71	0.92	60	4.00	*Adv. Mater.*, 2016 [6]
Cal-CoZIF-VXC72	0.84	5.92	--	35	4.00	*Adv. Mater.*, 2017 [7]
Co_3O_4/Co-N-C	0.91	5.10	0.98	68.5	3.62	*Journal of Power Sources*, 2017 [8]
Co/NPC	0.79	5.46	0.91	--	3.85~4.00	*J Mater Sci*, 2018 [9]
Co_3O_4/Co@N-G	0.81	5.20	0.96		3.91~3.96	*J. Mater. Chem. A*, 2019 [10]
Co@NPC/C-MWCNTs)	0.79	4.39	0.87	40.3	3.51	*Chemical Engineering Journal*, 2022 [11]
Co@NCNTs-700–2	0.81	7.4	0.89		3.92~4.13	*Journal of Alloys and Compounds*, 2022 [12]
Co-ZIF_x/CNF_y	0.85	2.96	0.93		4.00	*Journal of Colloid and Interface Science*, 2023 [13]
Co@NC	0.895	4.6		61	3.48	*Journal of Electroanalytical Chemistry*, 2023 [14]

References

1. Xia, W.; Zou, R.Q.; An, L.; Xia, D.G.; Guo, S.J. Metal-organic framework route to in-situ encapsulation of Co@Co_3O_4@C core@bishell nanoparticles into highly ordered porous carbon matrix for oxygen reduction. *Energy Environ. Sci.* **2015**, *8*, 568–576.
2. Zeng, M.; Liu, Y.L.; Zhao, F.P.; Nie, K.Q.; Han, N.; Wang, X.X.; Huang, W.J.; Song, X.N.; Zhong, J.; Li, Y.G. Metallic cobalt nanoparticles encapsulated in nitrogen enriched graphene shells: Its bifunctional electrocatalysis and application in Zinc–Air batteries. *Adv. Funct. Mater.*, **2016**, *26*, 4397–4404.
3. Li, X.Y.; Jiang, Q.Q.; Dou, S.; Deng, L.B.; Huo, J.; Wang, S.Y. ZIF-67-derived Co-NC@CoP-NC nanopolyhedra as an efficient bifunctional oxygen electrocatalyst. *J. Mater. Chem. A*, **2016**, 4, 15836–15840.
4. Wang, Z.; Li, B.; Ge, X.M.; Thomas Goh, F.W.; Zhang, X.; Du, G.J.; Wuu, D.; Liu, Z.L.; Andy Hor, T.S.; Zhang, H.; et al. Co@Co_3O_4@PPD core@bishell nanoparticle-based composite as an efficient electrocatalyst for oxygen reduction reaction. *Small* **2016**, *12*, 2580–2587.
5. Zhang, E.; Xie, Y.; Ci, S.Q.; Jia, J.C.; Cai, P.W.; Yi, L.C.; Wen, Z.H. Multifunctional high-activity and robust electrocatalyst derived from metal-organic frameworks. *J. Mater. Chem. A*, **2016**, *4*, 17288–17298.
6. Shang, L.; Yu, H.J.; Huang, X.; Bian, T.; Shi, R.; Zhao, Y.F.; Waterhouse, G.I.N.; Wu, L.Z.; Tung, C.H.; Zhang, T.R. Well-dispersed ZIF-derived Co,N-Co-doped carbon nanoframes through mesoporous-silica-protected calcination as efficient oxygen reduction electrocatalysts. *Adv. Mater.*, **2016**, *28*, 1668–1674.
7. Ni, B.; Ouyang, C.; Xu, X.B.; Zhuang, J.; Wang, X. Modifying commercial carbon with trace amounts of ZIF to prepare derivatives with superior ORR activities. *Adv. Mater.*, **2017**, *29*, 1701354.
8. Li, J.S.; Zhou, Z.; Liu, K.; Li, F.Z.; Peng, Z.G.; Tang, Y.G.; Wang, H.Y. Co_3O_4/Co-N-C modified ketjenblack carbon as an advanced electrocatalyst for Al-Air batteries. *J. Power Sources* **2017**, *343*, 30–38.
9. Zhan, T.R.; Lu, S.S.; Rong, H.Q.; Hou, W.G.; Teng, H.N.; Wen, Y.H. Metal-organic-framework-derived Co/nitrogen-doped porous carbon composite as an effective oxygen reduction electrocatalyst. *J. Mater. Sci.* **2018**, *53*, 6774–6784.
10. Guo, J.; Gadipelli, S.; Yang, Y.C.; Li, Z.N.; Lu, Y.; Brett, D.J.L.; Guo, Z.X. An efficient carbon-based ORR catalyst from low temperature etching of ZIF-67 with ultra-small cobalt nanoparticles and high yield. *J. Mater. Chem. A*, **2019**, *7*, 3544–3551.
11. He, H.; Lei, Y.X.; Liu, S.; Thummavichai, K.; Zhu, Y.Q.; Wang, N.N. ZIF-67-derived Co nanoparticles embedded in N-doped porous carbon composite interconnected by MWCNTs as highly efficient ORR electrocatalysts for a flexible direct formate fuel cell. *Chem. Eng. J.* **2022**, *432*, 134192.
12. Li, S.A.; Feng, C.; Xie, Y.H.; Guo, C.Y.; Zhang, L.G.; Wang, J.D. Synthesis of nitrogen-rich porous carbon nanotubes coated Co nanomaterials as efficient ORR electrocatalysts via MOFs as precursor. *J. Alloys Compd.* **2022**, *911*, 165060.
13. Liu, Z.F.; Ye, D.D.; Zhu, X.; Wang, S.L.; Zou, Y.N.; Lan, L.H.; Chen, R.; Yang, Y.; Liao, Q. Tunable active-sites of Co–nanoparticles encapsulated in carbon nanofiber as high performance bifunctional OER/ORR electrocatalyst. *J. Colloid Interface Sci.* **2023**, *630*, 140–149.
14. Chu, Y.; Jiang, Q.L.; Chang, L.Y.; Jin, Y.H.; Wang, R.Z. Cobalt nanoparticles embedded in nitrogen-doped porous carbon derived the electrodeposited ZnCo-ZIF for high-performance ORR electrocatalysts. *J. Electroanal. Chem.* **2023**, *928*, 117041.